JOC Article

A Theoretical Study of Reactivity and Regioselectivity in the Hydroxylation of Adamantane by Ferrate(VI)

Yoshihito Shiota, Naoki Kihara, Takashi Kamachi, and Kazunari Yoshizawa*

Institute for Fundamental Research of Organic Chemistry, Kyushu University, Fukuoka 812-8581, Japan

kazunari@ms.ifoc.kyushu-u.ac.jp

Received November 27, 2002

The conversion of adamantane to adamantanols mediated by ferrate (FeO_4^{2-}), monoprotonated ferrate ($HFeO_4^-$), and diprotonated ferrate (H_2FeO_4) is discussed with the hybrid B3LYP density functional theory (DFT) method. Diprotonated ferrate is the best mediator for the activation of the C−H bonds of adamantane via two reaction pathways, in which 1-adamantanol is formed by the abstraction of a tertiary hydrogen atom (3°) and 2-adamantanol by the abstraction of a secondary hydrogen atom (2°). Each reaction pathway is initiated by a C−H bond cleavage via an H-atom abstraction that leads to a radical intermediate, followed by a C−O bond formation via an oxygen rebound step to lead to an adamantanol complex. The activation energies for the C−H cleavage step are 6.9 kcal/mol in the 1-adamantanol pathway and 8.4 kcal/mol in the 2-adamantanol pathway, respectively, at the B3LYP/6-311++G** level of theory, whereas those of the second reaction step corresponding to the rebound step are relatively small. Thus, the rate-determining step in the two pathways is the C−H bond dissociation step, which is relevant to the regioselectivity for adamantane hydroxylation. The relative rate constant (3°)/(2°) for the competing H-atom abstraction reactions is calculated to be 9.30 at 75 °C, which is fully consistent with an experimental value of 10.1.

Introduction

Ferrate (FeO_4^{2-}) is considered to be an attractive alternative to frequently used oxidants such as potassium permanganate, potassium chromate, and potassium dichromate that are corrosive and violently toxic to human beings and to the environment.[1,2] The redox potentials of ferrate indicate that ferrate is thermodynamically a strong oxidant compared to MnO_4^- and $Cr_2O_7^{2-}$. The redox potentials between Fe(VI) and Fe(III) are +2.20 and +0.72 V in acidic and basic media, respectively,[3,4] whereas those of MnO_4^- ($Cr_2O_7^{2-}$) are +1.67 V (+1.33 V) in acidic media and +0.56 V (−0.12 V) in basic media. Since Hrostowski and Scott established the preparation method of potassium ferrate in 1950,[5] this high-valent transition-metal oxidant has been extensively studied because ferrate is relatively a mild oxidant for various organic compounds such as alcohols,[6,7] amines,[7] hydrazines,[8] peroxides,[9] and thiosulfates[8] with harmless wastes of $Fe(OH)_3$. Potassium ferrate can convert primary alcohols into aldehydes and secondary alcohols into ketones with excellent selectivity, whereas it does not react with tertiary alcohols.[10−12] In general, the solvent acidity must be carefully controlled in oxidation reactions mediated by ferrate to avoid a self-destruction of ferrate.[4] Ferrate is considerably stable in strongly alkaline solution around pH 10, whereas it decomposes spontaneously at a very rapid rate in acidic or neutral solution according to eq 1:

$$4FeO_4^{2-} + 10H_2O \rightarrow 4Fe(OH)_3 + 3O_2 + 8OH^- \quad (1)$$

The four oxygen atoms of ferrate are found from an experiment with isotope oxygen labeled ferrate[6] to be equivalent and exchangeable with solvent molecules, and the structure of FeO_4^{2-} is known from an X-ray crystallographic analysis to be slightly distorted from T_d symmetry.[13] Griffith demonstrated using IR spectroscopy that the mononuclear structure is retained in aqueous solution.[14]

The development of catalysts for the selective oxidation of saturated hydrocarbons is a central research subject in modern chemistry. Ferrate is expected to oxidize such inert hydrocarbons as well as alcohols. Delaude and

* To whom correspondence should be addressed.

(1) (a) *Oxidation in Organic Chemistry*; Wiberg, K. B., Ed.; Academic Press: New York, 1965; Part A. (b) *Oxidation in Organic Chemistry*; Trakanovsky, W. S., Ed.; Academic Press: New York, 1973; Part B. (c) *Comprehensive Organic Synthesis (Oxidation)*; Trost, B. M., Ed.; Pergamon: New York, 1991; Vol. 7.

(2) Spiro, T. G.; Stigliani, W. M. *Chemistry of the Environment*; Prentice Hall: Upper Saddle River, NJ, 1996.

(3) Wood, R. H. *J. Am. Chem. Soc.* **1958**, *80*, 2038.

(4) Sharma, V. K. *Adv. Environ. Res.* **2002**, *6*, 143.

(5) Hrostowski, H. J.; Scott, A. B. *J. Chem. Phys.* **1950**, *18*, 105.

(6) Tsuda, Y.; Nakajima, S. *Chem. Lett.* **1978**, 1397.

(7) (a) Johnson, M. D.; Hornstein, B. J. *Inorg. Chim. Acta* **1994**, *225*, 145. (b) Johnson, M. D.; Read, J. F. *Inorg. Chem.* **1996**, *35*, 6795.

(8) Goff, H.; Murmann, R. K. *J. Am. Chem. Soc.* **1971**, *93*, 6058.

(9) Delaude, L.; Laszlo, P.; Lehance, P. *Tetrahedron Lett.* **1995**, *36*, 8505.

(10) Williams, D. H.; Riley, J. T. *Inorg. Chim. Acta* **1974**, *8*, 177.

(11) Norcross, B. E.; Lewis, W. C.; Gai, H.; Noureldin, N. A.; Lee, D. G. *Can. J. Chem.* **1997**, *75*, 129.

(12) Huang, H.; Sommerfeld, D.; Dunn, B. C.; Eyring, E. M.; Lloyd, C. R. *J. Phys. Chem. A* **2001**, *105*, 3536.

(13) Hoppe, M. L.; Schlemper, E. O.; Murmann, R. K. *Acta Crystallogr.* **1982**, *B38*, 2237.

(14) Griffith, W. P. *J. Chem. Soc. A* **1966**, 1467.

10.1021/jo0207168 CCC: $25.00
Published on Web 04/11/2003

SCHEME 1

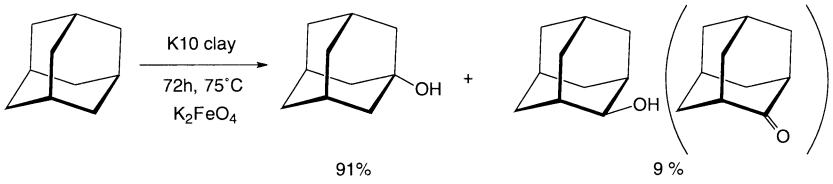

Laszlo[15] investigated adamantane hydroxylation by ferrate in the presence of K10 montmorillonite clay and demonstrated that adamantanols and adamantanone were obtained within 72 h at 75 °C (see Scheme 1). The products consist of 1-adamantanol (91%) and the mixture of 2-adamantanol and 2-adamantanone (9%). To the best of our knowledge, the reaction mechanism for this selective oxidation is still unknown.

Schröder, Schwarz, and co-workers have systematically investigated the gas-phase reactions of the bare FeO^+ ion and methane under ion cyclotron resonance conditions, demonstrating that FeO^+ is able to activate methane.[16] Theoretical studies of methane hydroxylation and related reactions by the bare FeO^+ complexes suggest two major reaction mechanisms that can be categorized by two kinds of H-atom abstractions from alkane.[17,18] One is a concerted H-atom abstraction via a four-centered transition state,[17] and the other is a direct H-atom abstraction via a transition state with a linear C−H−O array.[18] We calculated and analyzed the reaction pathway and energetics for methane hydroxylation by FeO^+, and demonstrated that the methane-to-methanol conversion should occur through an H-atom abstraction that involves a four-centered transition state. The direct benzene−phenol conversions by FeO^+ in the gas phase[19] and by an iron-oxo species over Fe-ZSM-5 zeolite[20] also take place in similar manners.

In a previous paper,[21] we investigated the C−H and O−H bond activation of methanol by ferrate with various density functional theory (DFT) methods. We proposed a favorable reaction pathway on the basis of potential energy surfaces and showed the C−H bond cleavage is initiated by a direct H-atom abstraction. No theoretical analysis of alkane hydroxylation by ferrate has been performed, probably due to the difficulty in modeling the actual active oxidant. In this article, we discuss possible mechanisms for the adamantane-to-adamantanol conversions by ferrate and protonated ferrates and reveal a novel oxidation ability of this species from a theoretical point of view.

Method of Calculation

We optimized local minima and saddle points on potential energy surfaces using the B3LYP method,[22,23] which has been reported to provide excellent descriptions of various reaction profiles, particularly in geometries, heats of reaction, barrier heights, and vibrational analyses.[24] For the Fe atom we used the (14s9p5d) primitive set of Wachters[25] supplemented with one polarization f-function ($\alpha = 1.05$ for Fe)[26] and for the carbon, oxygen, and hydrogen atoms we used the 6-311G** basis set,[27] a triple-ζ basis set with polarization functions. All the geometries for the reaction species and transition states were fully optimized without symmetry constraint. After geometry optimizations at the B3LYP/6-311G** level, we carried out single-point calculations at the B3LYP/6-311++G** level (B3LYP/6-311++G**//B3LYP/6-311G**). We used 1s2p1d functions for the iron atom,[28] one sp-function for the carbon and oxygen atoms, and one s-function for the hydrogen atom as additional diffuse functions.[29] The spin-unrestricted version of the B3LYP (UB3LYP) method was applied even to singlet states when the reaction species are reasonably considered to have an open-shell-singlet electronic configuration. Computed $\langle S^2 \rangle$ values[30] suggested that almost no spin contamination is included in the calculations except in open-shell-singlet calculations. We performed systematic vibrational analyses at the B3LYP/6-311G** level of theory to confirm that an optimized geometry corresponds to a transition state that has only one imaginary frequency or a local minimum that has no imaginary frequency. We took zero-point-energy corrections into account in calculating the energetics of the reaction pathways. We used the Gaussian 98 program package[31] for the calculations.

(15) Delaude, L.; Laszlo, P. *J. Org. Chem.* **1996**, *61*, 6360.
(16) Schröder, D.; Schwarz, H. *Angew. Chem., Int. Ed. Engl.* **1990**, *29*, 1433.
(17) (a) Yoshizawa, K.; Shiota, Y.; Yamabe, T. *Chem. Eur. J.* **1997**, *3*, 1160. (b) Yoshizawa, K.; Shiota, Y.; Yamabe, T. *J. Am. Chem. Soc.* **1998**, *120*, 564. (c) Yoshizawa, K.; Shiota, Y.; Yamabe, T. *J. Chem. Phys.* **1999**, *111*, 538. (d) Yoshizawa, K.; Shiota, Y.; Kagawa, Y.; Yamabe, T. *J. Phys. Chem. A* **2000**, *104*, 2552. (e) Yoshizawa, K.; Kagawa, Y. *J. Phys. Chem. A* **2000**, *104*, 9347. (f) Shiota, Y.; Yoshizawa, K. *J. Am. Chem. Soc.* **2000**, *122*, 12317. (g) Yumura, T.; Yoshizawa, K. *Organometallics* **2001**, *20*, 1397. (h) Yumura, T.; Amenomori, T.; Kagawa, Y.; Yoshizawa, K. *J. Phys. Chem. A* **2002**, *106*, 621.
(18) Yoshizawa, K.; Shiota, Y.; Yamabe, T. *Organometallics* **1998**, *17*, 2825.
(19) Yoshizawa, K.; Shiota, Y.; Yamabe, T. *J. Am. Chem. Soc.* **1999**, *121*, 147.
(20) (a) Yoshizawa, K.; Yumura, T.; Shiota, Y.; Yamabe, T. *Bull. Chem. Soc. Jpn.* **2000**, *73*, 29. (b) Yoshizawa, K.; Shiota, Y.; Yumura, T.; Yamabe, T. *J. Phys. Chem. B* **2000**, *104*, 734.
(21) Ohta, T.; Kamachi, T.; Shiota, Y.; Yoshizawa, K. *J. Org. Chem.* **2001**, *66*, 4122.
(22) (a) Becke, A. D. *Phys. Rev. A* **1988**, *38*, 3098. (b) Becke, A. D. *J. Chem. Phys.* **1993**, *98*, 5648.
(23) Lee, C.; Yang, W.; Parr, R. G. *Phys. Rev. B* **1988**, *37*, 785.
(24) (a) Baker, J.; Muir, M.; Andzelm, J.; Scheiner, A. In *Chemical Applications of Density-Functional Theory*; Laird, B. B., Ross, R. B., Ziegler, T., Eds.; ACS Symp. Ser. No. 629; American Chemical Society: Washington, DC, 1996. (b) Koch, W.; Holthausen, M. C. *A Chemist's Guide to Density Functional Theory*; Wiley-VCH: Weinheim, Germany, 2000.
(25) Wachters, A. J. H. *J. Chem. Phys.* **1970**, *52*, 1033.
(26) Raghavachari, K.; Trucks, G. W. *J. Chem. Phys.* **1989**, *91*, 1062.
(27) Raghavachari, K.; Binkley, J. S.; Seegar, R.; Pople, J. A. *J. Chem. Phys.* **1980**, *72*, 650.
(28) Hay, P. J. *J. Chem. Phys.* **1977**, *66*, 4377.
(29) Clark, T.; Chandrasekhar, J.; Spitznagel, G. W.; Schleyer, P. v. R. *J. Comput. Chem.* **1983**, *4*, 294.
(30) Wang, J.; Becke, A. D.; Smith, V. H., Jr. *J. Chem. Phys.* **1995**, *102*, 3477.
(31) Frisch, M. J.; Trucks, G. W.; Schlegel, H. B.; Scuseria, G. E.; Robb, M. A.; Cheeseman, J. R.; Zakrzewski, V. G.; Montgomery, J. A.; Stratmann, R. E.; Burant, J. C.; Dapprich, S.; Millam, J. M.; Daniels, A. D.; Kudin, K. N.; Strain, M. C.; Farkas, O.; Tomasi, J.; Barone, V.; Cossi, M.; Cammi, R.; Mennucci, B.; Pomelli, C.; Adamo, C.; Clifford, S.; Ochterski, J.; Petersson, G. A.; Ayala, P. Y.; Cui, Q.; Morokuma, K.; Malick, D. K.; Rabuck, A. D.; Raghavachari, K.; Foresman, J. B.; Cioslowski, J.; Ortiz, J. V.; Stefanov, B. B.; Liu, G.; Liashenko, A.; Piskorz, P.; Komaromi, I.; Gomperts, R.; Martin, R. L.; Fox, D. J.; Keith, T.; Al-Laham, M. A.; Peng, C. Y.; Nanayakkara, A.; Gonzalez, C.; Challacombe, M.; Gill, P. M. W.; Johnson, B. G.; Chen, W.; Wong, M. W.; Andres, J. L.; Head-Gordon, M.; Replogle, E. S.; Pople, J. A. *Gaussian 98*; Gaussian Inc.: Pittsburgh, PA, 1998.

CHART 1

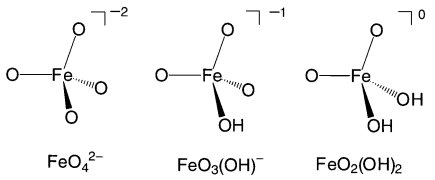

Results and Discussion

1. Ferrate Models. Since protonated ferrate is experimentally known to exhibit stronger oxidation ability, we considered ferrate and protonated ferrates as active species models, as shown in Chart 1, and revealed that diprotonated ferrate can activate the C−H and O−H bonds of methanol whereas ferrate and monoprotonated ferrate are not effective for methanol oxidation.[21] We carried out DFT calculations at the B3LYP level of theory to determine the actual active species of alkane hydroxylation by ferrate, which can cleave the C−H bonds of adamantane, and concluded that only diprotonated ferrate can activate the C−H bonds of adamantane, whereas ferrate and monoprotonated ferrate are unable to activate adamantane.

This difference in reactivity among ferrate and protonated ferrates would derive from the difference in the spin distribution in these species. The produced hydroxo ligands in mono- and diprotonated ferrate have no spin density; thus, the protonation of the oxo ligands of ferrate increases the spin density of the remaining oxo ligands after reconstruction of the four Fe−O bonds. In contrast, the spin density of the iron atom remains almost unchanged because the d orbitals of the iron atom are not significantly affected by the protonation. Therefore such an increase in the spin density of an oxo ligand causes the H-atom abstraction from an inert C−H bond of hydrocarbon as well as that of methanol, whereas a hydroxo ligand produced by the protonation of an oxo ligand has no reactivity to the H-atom abstraction. Considering these spin densities and charge effects, diprotonated ferrate is likely to be the strongest oxidant among these ferrates and can effectively mediate the hydroxylation of adamantane.

K10 montmorillonite clay, a catalyst for adamantane hydroxylation by ferrate, is generally considered to act as a host material[32] that induces an encounter with substrates. Our calculations suggest an overlooked role of this catalyst as a proton donor in aprotic solvent. Although dried K10 clay has limited reactivity in cyclohexane oxidation, air moisture greatly increases its catalytic activity for oxidation.[15] We assume from the experimental results that moist K10 clay provides a number of water molecules to generate diprotonated ferrate. Recently, Ho and Lau[33] reported that the coordination of an oxo ligand of ferrate to a Lewis acid enhances its oxidation ability, due to the withdrawal of electron density from the oxo ligand by the metal ion that acts as a Lewis acid. The Lewis acid−$BaFeO_4$ system can

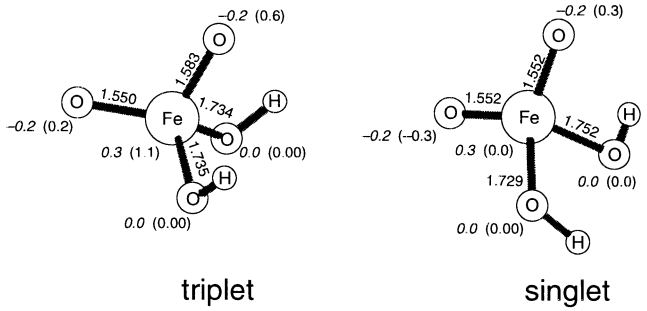

FIGURE 1. Optimized structures and charges (italic) of diprotonated ferrate. The values in parentheses are spin densities. Bond distances are in Å.

oxidize small alkanes such as ethane and propane at room temperature. These experimental results indicate that some activation process of ferrate (FeO_4^{2-}) is necessary to promote alkane hydroxylation.

The optimized structure of diprotonated ferrate in the triplet state has a close resemblance to that in the singlet state, as shown in Figure 1. These bond distances between the Fe and O atoms were calculated to be about 1.55 Å in the oxo ligand and 1.73 Å in the hydroxo ligand. In the triplet state the oxo ligand with a spin density of +0.6 leads to the H-atom abstraction, whereas the other oxo ligand and the hydroxo ligands are not expected to mediate it because these ligands are not a spin carrier. In the singlet state the spin densities of the two oxo ligands are +0.3 and −0.3, and that of the iron atom is 0. Therefore our DFT calculations predict that the two oxo ligands can mediate the H-atom abstraction in the singlet state.

2. Energy Diagrams. We found possible reaction pathways for adamantane hydroxylation by diprotonated ferrate, as shown in Scheme 2. The reactions give two different products: path 1 leads to the formation of 1-adamantanol via a radical intermediate that has a tertiary carbon radical, and path 2 leads to the formation of 2-adamantanol via a radical intermediate that has a secondary carbon radical. Let us look at computed potential energy profiles along the reaction pathways before detailed commentary on these reaction species. Figure 2 shows computed energy diagrams for path 1 and path 2 in the triplet state. The hydroxylation reaction by diprotonated ferrate starts from the formation of the reactant complex in which adamantane is weakly bound to the ferrate with a binding energy of 0.6 kcal/mol. This small value is reasonable for the binding energy between the neutral iron-oxo species and alkane: 5.7 (FeO and methane),[18] 0.9 (P450 and ethane),[34a] 3.1 (P450 and camphor),[34b] and 3.4 kcal/mol (α-oxygen model of Fe-ZSM-5 and methane).[20b]

The direct H-atom abstractions from the tertiary and secondary carbon atoms of adamantane occur in **^{3}TS1-3** and **^{3}TS1-2**, leading to the radical intermediates **^{3}Int-3** and **^{3}Int-2**, respectively. Calculated activation energies of 6.9 kcal/mol for **^{3}TS1-3** and of 8.4 kcal/mol for **^{3}TS1-2** are lower than those for other oxo species, 23.5 kcal/mol

(32) (a) Stucki, J. W. *Iron in Soils and Clay Minerals*; Stucki, J. W., Goodman, B. A., Schwertmann, U., Eds.; D. Reidel: Dordrecht, The Netherlands, 1988; p 625. (b) Stucki, J. W. *Advances in GeoEcology*; Auerswald, K., Stanjek, H., Eds.; Catena-Verlag: Amsterdam, The Netherlands, 1997; Vol. 30, p 395.

(33) Ho, C.-M.; Lau, T.-C. *New J. Chem.* **2000**, *24*, 587.

(34) (a) Yoshizawa, K.; Kagawa, Y.; Shiota, Y. *J. Phys. Chem. B* **2000**, *104*, 12365. (b) Kamachi, T.; Yoshizawa, K. *J. Am. Chem. Soc.* **2003**, *125*, in press.

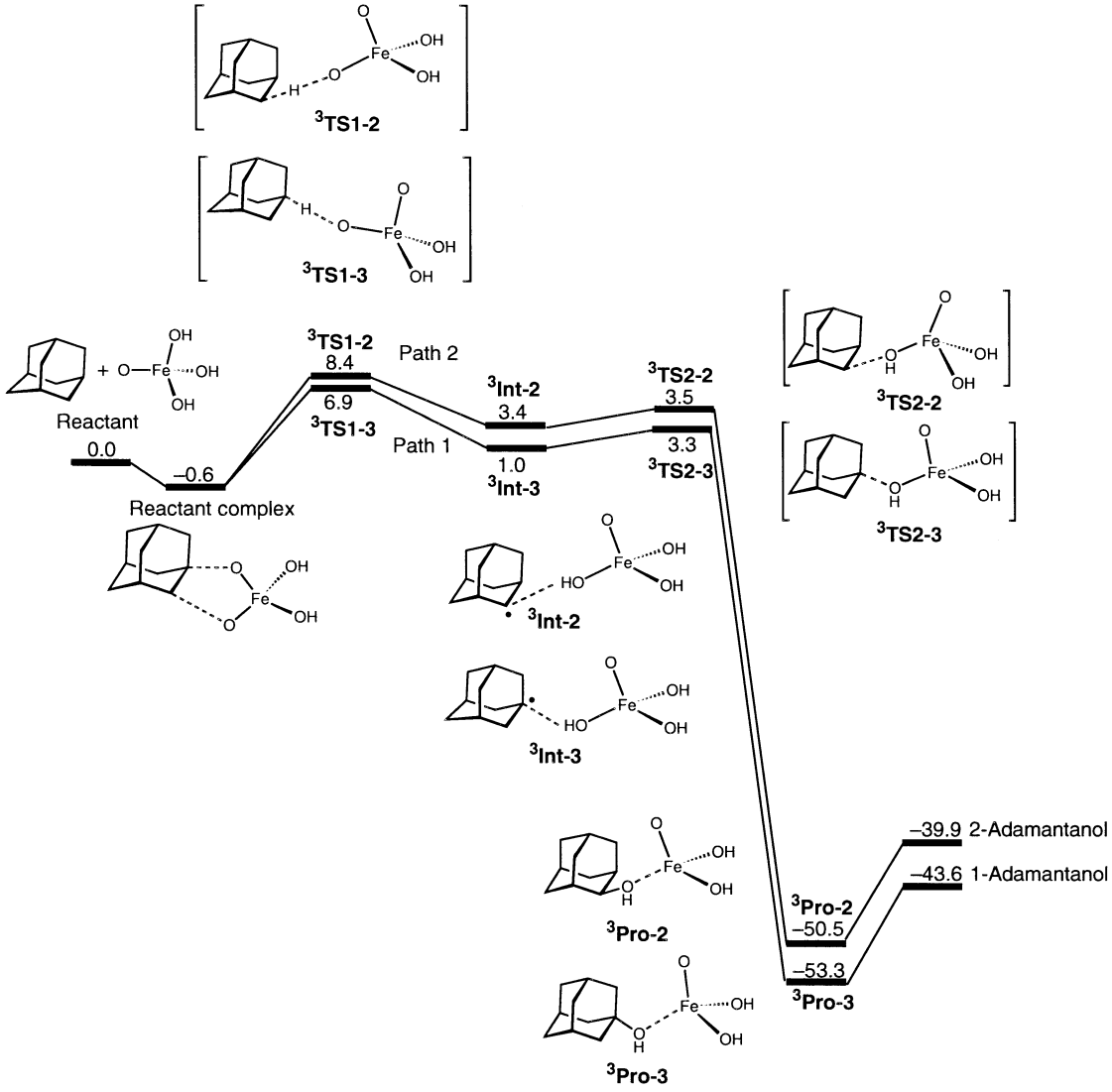

FIGURE 2. Potential energy diagram in the triplet state. Units are in kcal/mol.

SCHEME 2

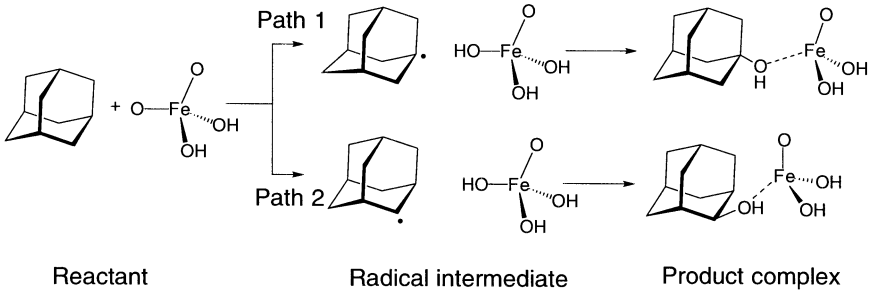

for FeO^+,[18] and 22.0 kcal/mol for ethane hydroxylation by compound I of cytochrome P450.[34a] These results suggest that diprotonated ferrate is a powerful oxidant for the cleavage of a C−H bond of adamantane. The potential energies of ^{3}**Int-3** and ^{3}**Int-2** are 1.0 and 3.4 kcal/mol relative to the dissociation limit (diprotonated ferrate + adamantane), respectively. The activation energies for the oxygen rebound step ^{3}**TS2-3** (^{3}**TS2-2**) are only 2.3 (0.1) kcal/mol relative to the radical intermediate ^{3}**Int-3** (^{3}**Int-2**). Thus, the radical intermediates easily go to the product complexes via the rebound steps, and each step is a downhill process with an exothermal energy of nearly 50 kcal/mol. This thermal energy derived from the formation of a C−O bond can promote the release of adamantanol from the product complex with a barrier of 9.7 kcal/mol in ^{3}**Pro-3** and 10.6 kcal/mol in ^{3}**Pro-2**. Our results predict that the total exothermic energies for the adamantane hydroxylations are 43.6 kcal/mol in 1-adamantanol and 39.9 kcal/mol in 2-adamantanol.

Let us next compare the electronic configurations and the energetic features between the singlet and triplet states to increase our understanding of the reaction

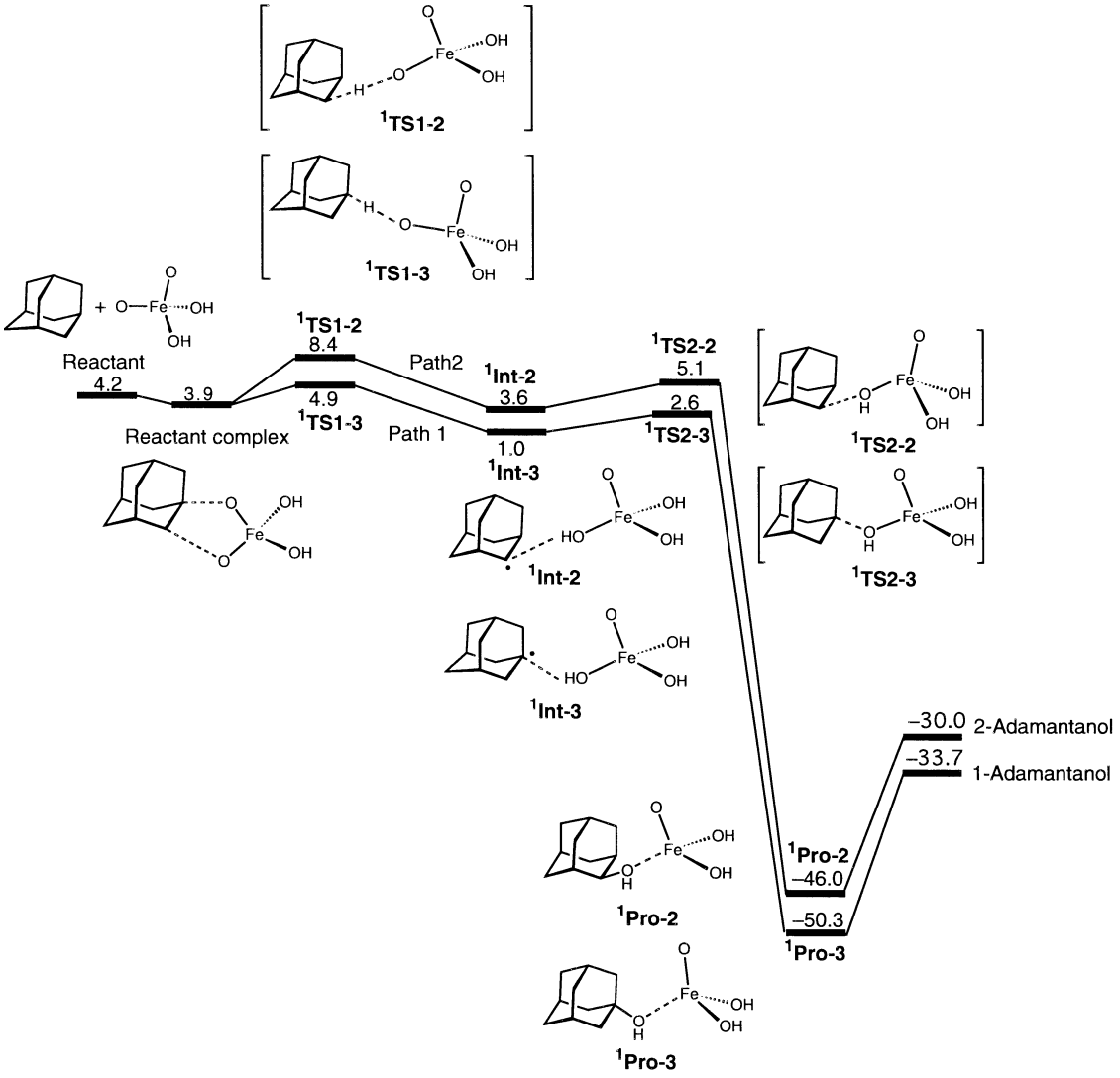

FIGURE 3. Potential energy diagram in the singlet state. Units are in kcal/mol.

mechanism. It is difficult to describe the singlet potential energy surface within the framework of the spin-restricted method because the diprotonated ferrate should have a d^2 electronic configuration, and we cannot reasonably impose a closed-shell electronic configuration on such an open-shell system. We therefore carried out open-shell-singlet calculations along the reaction pathways (path 1 and path 2) with the spin-unrestricted version of the B3LYP method (UB3LYP), as depicted in Figure 3. To check the broken-symmetry calculations, we summarized calculated spin densities of the triplet and singlet states in Table 1. The calculated potential energy surface of this hydroxylation reaction in the open-shell-singlet state is close to that in the triplet state. In particular, the relative energies of **Int-3** in both spin states are similar because the 1-adamantyl radical has a weak interaction with the iron center of ferrate. The crossing of the different spin multiplicity surfaces occurs just before **TS1**: ^{3}**TS1-3** lies 2.0 kcal/mol above ^{1}**TS1-3**, which leads to a small decrease (2.0 kcal/mol) in the barrier height of **TS1**. However, the favorable reaction pathway of the singlet state is essentially identical with that of the triplet state. Note that the rate-determining step in the singlet state is also the C−H bond dissociation step and the singlet potential energy surface of path 1 always lies below that of path 2. Therefore the spin-forbidden crossing has no influence on the reactivity and regioselectivity in adamantane hydroxylation. A spin-forbidden transition requires an effect of spin−orbit coupling that provides the major mechanism for intersystem crossing.[35] Since the observed effective magnetic

TABLE 1. Calculated Spin Densities for the Iron Atom and the Oxygen Atom[a,b] and the Carbon Radical Center in the Triplet State[c]

	Fe	O[a,b]	C
reactant complex	1.1 (0.0)	0.6, 0.2 (−0.2, 0.2)	0.0 (0.0)
TS1-2	0.8 (0.6)	0.4 (−0.4)	0.4 (−0.4)
TS1-3	0.8 (0.6)	0.5 (−0.3)	0.3 (−0.3)
Int-2	0.8 (0.8)	0.1 (0.0)	1.0 (−1.0)
Int-3	0.8 (0.7)	0.1 (0.0)	0.8 (−0.8)
TS2-2	1.1 (0.5)	−0.1 (0.1)	0.9 (−0.9)
TS2-3	1.2 (0.3)	0.0 (0.1)	0.6 (−0.6)
Pro-2	1.6 (0.3)	0.0 (0.0)	0.0 (0.0)
Pro-3	1.6 (0.4)	0.0 (0.0)	0.0 (0.0)

[a] Two oxo ligands of the reactant complex are indicated. [b] One oxygen atom is related to the reactions that abstract the hydrogen in **TS1** and form the C−O bond in **TS2**. [c] The values in the parentheses are spin densities in the singlet state.

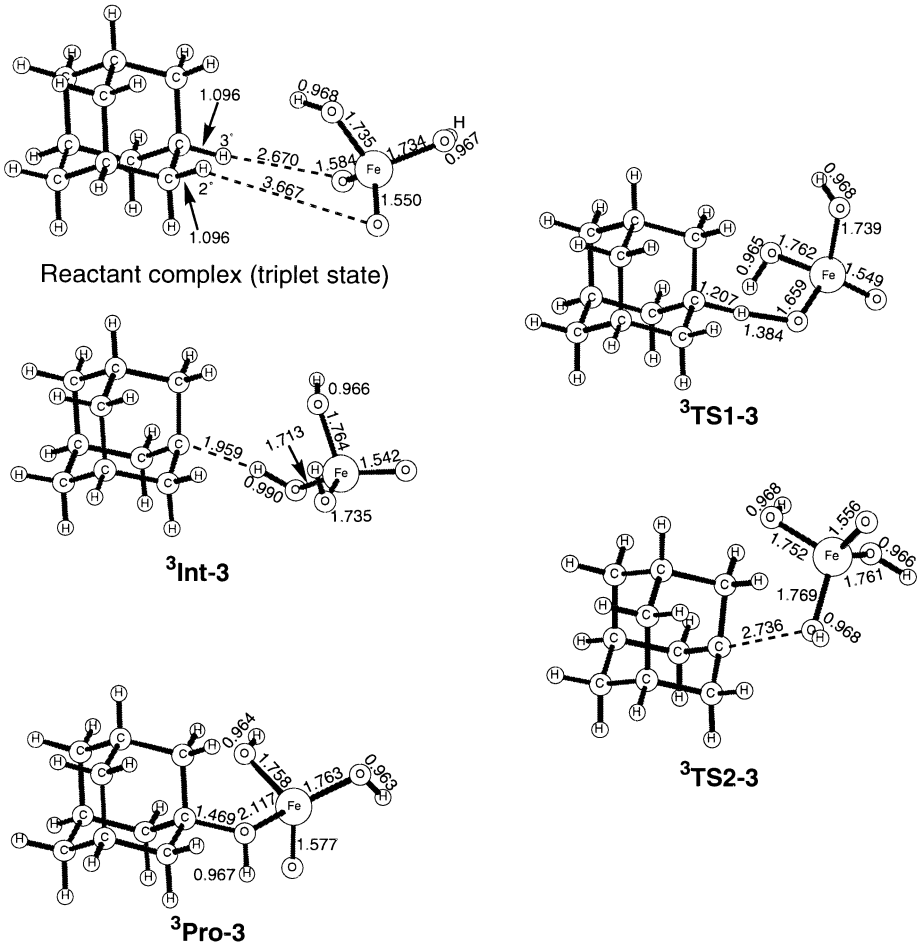

FIGURE 4. Optimized structures of reactant, transition states, intermediate, and product along path 1 in the triplet state. Bond distances are in Å.

moment of ferrate[36] indicates the singlet−triplet spin−orbit coupling cannot be significant, we do not consider that the spin-inversion process plays an essential role in the reaction. Thus, we focused on the triplet energy profile in the present study.

3. Optimized Structures. We show in Figure 4 optimized geometries for the reaction species along path 1 in the triplet state. To avoid duplication of discussion, those in the singlet state are depicted in the Supporting Information. In the reactant complex diprotonated ferrate and adamantane moieties are geometrically similar to each isolated structure and the total charge of the ferrate moiety is only +0.06. This similarity indicates that the reactant complex has only a weak interaction between diprotonated ferrate and adamantane. These results are consistent with a small binding energy of 0.6 kcal/mol. This weak binding allows reorientation of the substrate in the reactant complex, resulting in a change from bidentate to monodentate coordination in going from the reactant complex to the transition state for the H-atom abstraction. The minimum distance between the oxo ligand and the hydrogen atom connected to a tertiary (secondary) carbon of adamantane is 2.670 Å (3.667 Å). Therefore the structure of the reactant complex is irrelevant to the regioselectivity of the H-atom abstraction from a tertiary or secondary carbon atom.

The dissociation of a tertiary C−H bond occurs in **^{3}TS1-3**, which exhibits a nearly linear C−H−O array with an imaginary vibrational frequency of 603*i* cm^{-1}, as expected from a general radical mechanism. The C−H bond distance of 1.207 Å and the O−H bond distance of 1.384 Å in the bond-cleavage and -creation regions of this transition state are quite reasonable. The Fe−O distance of 1.659 Å in **^{3}TS1-3** is slightly longer than that of the reactant complex (1.584 Å), although the other Fe−O distances remain almost unchanged during this hydrogen shift. The resultant radical intermediate **^{3}Int-3** has a large spin density of +0.8 on the carbon radical center of the 1-adamantyl radical that is weakly bonded to a hydroxo ligand of ferrate with a distance of 1.959 Å. The radical intermediate **^{3}Int-3** is transformed into the product complex via a transition state (**^{3}TS2-3**) in which a C−O bond formation occurs. This transition state has an imaginary frequency of 481*i* cm^{-1} that corresponds to C−O stretching, and it connects the radical intermediate and the product complex. The Fe−O bond distances increase from 1.769 Å in **^{3}TS2-3** to 2.117 Å in **^{3}Pro-3**. The large spin density on the radical center of **^{3}Int-3** disappears in the product complex, due to the formation of the C−O bond, and the spin density of the iron center

(35) (a) Lower, S. K.; El-Sayed, M. A. *Chem. Rev.* **1966**, *66*, 199. (b) Salem, L.; Rowland, C. *Angew. Chem., Int. Ed. Engl.* **1972**, *11*, 92.

(36) (a) Audette, R. J.; Quail, J. W.; Smith, P. J. *Tetrahedron Lett.* **1971**, 279. (b) Audette, R. J.; Quail, J. W. *Inorg. Chem.* **1972**, *11*, 1904.

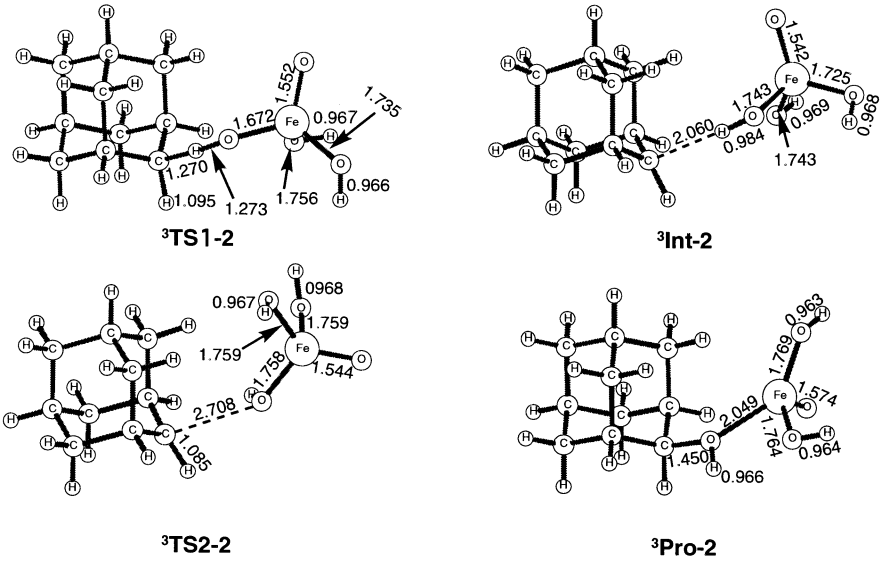

FIGURE 5. Optimized structures of transition states, intermediate, and product along path 2 in the triplet state. Bond distances are in Å.

increases from +0.8 to +1.6. The release of 1-adamantanol from ^{3}**Pro-3** leads to the final complex, $FeO(OH)_3$.

Let us next look at a calculated reaction pathway for the formation of 2-adamantanol. Figure 5 shows optimized structures of the transition states, intermediate, and product along path 2. The optimized structure of ^{3}**TS1-2** with an imaginary frequency of 1234*i* cm^{-1} seems to be reasonable for the cleavage of a C−H bond. The C−H and O−H bond distances in this transition state are 1.270 and 1.273 Å, respectively. The radical intermediate ^{3}**Int-2** consists of the 2-adamantyl radical and $FeO(OH)_3$ and has a spin density of +1.0 on the carbon radical center with a planar structure in contrast to the 1-adamantyl radical in which the carbon radical center is not planar due to the constraint of the adamantane framework. The recombination between a hydroxo ligand of the ferrate and the 2-adamantyl radical occurs in ^{3}**TS2-2**, leading to the product complex ^{3}**Pro-2** that involves 2-adamantanol as a ligand. ^{3}**TS2-2** is a transition state with an imaginary frequency of 196*i* cm^{-1} along the reaction pathway. The C−O distance of 2.708 Å in ^{3}**TS2-2** decreases to 1.450 Å in the product complex.

4. Relative Rate, Regioselectivity, and Isotope Effect. Let us finally compare the energetics of the two reaction pathways (path 1 and path 2) from the viewpoint of regioselectivity and isotope effect. As we saw, 1-adamantanol is formed by the abstraction of a tertiary hydrogen atom, and 2-adamantanol by the abstraction of a secondary hydrogen atom. Since the transition state for the C−H bond dissociation lies in energy above that for the rebound step, the rate-determining step for path 1 and path 2 is the C−H bond dissociation step, being relevant to the regioselectivity in adamantane hydroxylation. Figure 2 shows that path 1 always lies a few kilocalories per mole below path 2, which is consistent with the experimental result that the main product is 1-adamantanol.

To refine our discussion for the regioselectivity, we considered the temperature dependence of the C−H bond dissociation rate that controls the regioselectivity in adamantane hydroxylation. We calculated the relative rate constant (k_1/k_2) for the competing H-atom abstraction reactions using transition-state theory[37] with eq 2,

$$\frac{k_1}{k_2} = \frac{4}{12}\frac{(I_x^1 I_y^1 I_z^1)^{1/2}}{(I_x^2 I_y^2 I_z^2)^{1/2}}\frac{q_v^1}{q_v^2}\exp\left(-\frac{E_1^{\#} - E_2^{\#}}{RT}\right) \qquad (2)$$

Here I and q are the moment of inertia and the vibrational partition function of the transition state, respectively. The superscripts 1 and 2 correspond to path 1 and path 2, respectively. $E^{\#}$ is the activation energy that includes zero-point energies and thermal corrections. The last exponential term is dominant in this equation because the other terms can be almost all canceled between denominators and numerators. The numerators in the last exponential term come from the fact that **TS1-3** has a lower activation energy than **TS1-2**. Since there are 4 tertiary and 12 secondary hydrogen atoms in adamantane, we consider the collision frequency of the hydrogen atom in the first term to estimate the substantial rate. Calculated rate constants (k_1/k_2) range from 8 to 20 at temperatures from 0 to 100 °C, as shown in Table 2. Thus, the relative rate constants suggest adamantane is attacked mainly on the tertiary carbons. The experimental result shows that the product branching-ratio is 1-adamantanol (91%) and the mixture of 2-adamantanol and 2-adamantanone (9%) at 75 °C.[15] The calculated rate constant (k_1/k_2) was 9.30 at 75 °C, which is in good

TABLE 2. Computed (k_1/k_2) Values[a] in the C−H Bond Dissociation of Adamantane by Diprotonated Ferrate

temp (°C)	k_1/k_2
0	19.5
25	14.6
50	11.5
75	9.30
100	7.76

[a] All energies are used at the B3LYP/6-311G** level.

(37) Frost, A. A.; Pearson, R. G. *Kinetics and Mechanism*; Wiley: New York, 1961.

agreement with the experimental value of 10.1.[15] This result supports that the H-atom abstraction step is the rate-determining step of adamantane hydroxylation by ferrate. Our calculations successfully reproduce the complicated chemical processes between adamantane and ferrate. Adamantane is a widely used substrate, which can tell us (3°)/(2°) regioselectivity in oxidizing catalysts. For example, cytochrome P450 and its model complex display high regioselectivity to this substrate (100% for $P450_{cam}$,[38] 91% for $P450_{LM2}$,[38] and 92% for tetraphenylporphinatoiron).[39] Non-heme iron catalysts such as Fe^{II}(TPA) complexes can also hydroxylate adamantane with H_2O_2, and these hydroxylations result in the 1-adamantanol branching ratio being in the range of 83−92%.[40] Thus, adamantane hydroxylation by ferrate can essentially be described in terms of the well-known "radical C−H activation/oxygen rebound" mechanism.

We carried out single-point calculations about important transition states to look at solvent effects using the polarized continuum model[41] with dielectric constant $\epsilon = 2.228$ (CCl_4). The relative energy of **TS1-2** (**TS1-3**) is changed from 8.4 (6.9) to 8.3 (6.5) kcal/mol. Since the branching ratio mainly depends on the energy difference between the two TSs, our computational results suggest that the external media does not significantly affect the 1-adamantanol branching ratio.

We finally performed kinetic isotope effect (KIE) calculations to better understand the reaction mechanism for the conversion of adamantane to adamantanols. KIE (k_H/k_D) is an important measure in discussing how the electronic process for H-atom abstraction from substrate hydrocarbon takes place in catalytic and enzymatic reactions. KIE is obtained by transition state theory[37] with eq 3.

$$k_H/k_D = \frac{(m_D^R m_H^\#)^{3/2}}{(m_H^R m_D^\#)^{3/2}} \frac{(I_{x_D}^R I_{y_D}^R I_{y_D}^R)^{1/2}}{(I_{x_H}^R I_{y_H}^R I_{z_H}^R)^{1/2}} \frac{(I_{x_H}^\# I_{y_H}^\# I_{z_H}^\#)^{1/2}}{(I_{x_D}^\# I_{y_D}^\# I_{y_D}^\#)^{1/2}} \frac{q_{vD}^R}{q_{vH}^R} \frac{q_{vH}^\#}{q_{vD}^\#} \exp\left(-\frac{E_H^\# - E_D^\#}{RT}\right) \quad (3)$$

Here m, I, q, and E indicate the molecular mass, the moment of inertia, the vibrational partition function, and the activation energy, respectively. Superscript R specifies adamantane and superscript # indicates the transition state. Subscript H means the species including $C_{10}H_{16}$ and subscript D means the species including $C_{10}D_{16}$. Calculated k_H/k_D values at 75 °C are 3.70 for 1-adamantanol and 5.83 for 2-adamantanol. Thus, the KIEs are dependent on site. If the direct C−H bond cleavage is really operative in the entrance reaction channel of adamantane oxidation by ferrate, we expect that the KIE value will be measured as approximately 4.

TABLE 3. Computed KIE (k_H/k_D) Values[a] in the C−H (C−D) Bond Dissociation of Adamantane by Diprotonated Ferrate

temp (°C)	^{3}TS1-2	^{3}TS1-3
0	10.8	5.16
25	8.59	4.55
50	6.99	4.08
75	5.83	3.70
100	4.95	3.40

[a] All energies are used at the B3LYP/6-311G** level.

Summary

We demonstrated using B3LYP/6-311++G**//B3LYP/6-311G** level calculations that diprotonated ferrate is the best mediator for the activation of the C−H bonds of adamantane via two reaction pathways: (1) 1-adamantanol is formed by the abstraction of a tertiary hydrogen atom; (2) 2-adamantanol is formed by the abstraction of a secondary hydrogen atom. These processes are two-step reactions. The first transition state corresponds to an H-atom abstraction, resulting in the formation of the radical intermediate that involves the adamantyl radical. The second transition state for the rebound step involves the formation of a C−O bond. The activation barriers for the C−H bond dissociation are 6.9 kcal/mol at the tertiary site (3°) and 8.4 kcal/mol at the secondary site (2°). Calculated potential energy surfaces suggest that the H-atom abstraction is the rate-determining step in these hydroxylations and is responsible for the regioselectivity in both reaction pathways. The formation of the tertiary adamantyl radical is energetically more favorable than the formation of the secondary adamantyl radical. This conclusion is fully consistent with the experimental result for the product branching ratio (91% 1-adamantanol and 9% 2-adamantanol + 2-adamantanone).[15] We finally analyzed using transition state theory the temperature dependence of the C−H bond dissociation rate of the two reaction pathways. The calculated relative rate constant (3°)/(2°) of 9.30 at 75 °C is in good agreement with an experimental value of 10.1.[15]

Acknowledgment. K.Y. acknowledges the Ministry of Culture, Sports, Science and Technology of Japan, the Japan Society for the Promotion of Science, the Iwatani Naoji Foundation, the Takeda Science Foundation, and Kyushu University P & P 'Green Chemistry' for their support of this work. Computations were in part carried out at the Computer Center of the Institute for Molecular Science.

Supporting Information Available: Optimized geometries of all the reaction species. This material is available free of charge via the Internet at http://pubs.acs.org.

JO0207168

(38) White, R. E.; McCarthy, M.-B.; Egeberg, K. D.; Sligar, S. G. *Arch. Biochem. Biophys.* **1984**, *228*, 493.
(39) Groves, J. T.; Nemo, T. E.; Myers. R. S. *J. Am. Chem. Soc.* **1979**, *101*, 1032.
(40) Chen, K.; Que, L., Jr. *J. Am. Chem. Soc.* **2001**, *123*, 6327.
(41) (a) Miertus, S.; Scrocco, E.; Tomasi, J. *Chem. Phys.* **1981**, *55*, 117. (b) Miertus, S.; Tomasi, J. *J. Chem. Phys.* **1982**, *65*, 239. (c) Barone, V.; Cossi, M.; Tomasi, J. *J. Chem. Phys.* **1997**, *107*, 3210. (d) Cossi, M.; Barone, V.; Cammi, R.; Tomasi, J. *Chem. Phys. Lett.* **1996**, *225*, 327.